ASMS

RESEARCH ARTICLE

An Orbital Trap Mass Analyzer Using a Hybrid Magnetic-Electric Field: A Simulation Study

Chongsheng Xu,[1] Fangling Wu,[1] Li Ding,[2] Chuan-Fan Ding[1]

[1]Department of Chemistry and Laser Chemistry Institute, Fudan University, 220 Handan Road, Shanghai, 200433, China
[2]Shimadzu Research Laboratory (Europe) Ltd., Wharfside, Trafford Wharf Road, Manchester, M17 1GP, UK
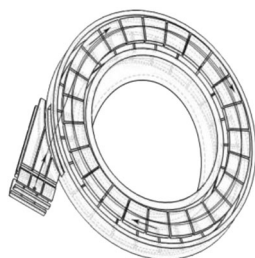
Abstract. An orbital ion trap mass analyzer employing hybrid magnetic-electric field was designed and simulated. The trap has a rotational symmetrical structure and the hybrid trapping field was created in a toroidal space between 12 pairs of sector detection electrodes. Ion injection and ion orbital motion inside the trap were simulated using SIMION 8.1 with a user Lua program, and the required electric and magnetic field were investigated. The image charge signal can be picked up by the 12 pairs of detection electrodes and the mass resolution was evaluated using FFT. The simulated resolving power for the optimized configuration over 79,000 FWHM was obtained at the magnetic induction intensity of 0.5 Tesla in the simulation.

Keywords: Orbital trap, Magnetic-electric field, Simulation, Fourier transform, High resolution, Mass analyzer

Introduction

Mass spectrometers based on ion motion in magnetic field have been widely used in chemistry, physics, geo-science, and biological research. From the traditional magnetic sector mass spectrometer to the Fourier transform ion cyclotron resonance mass spectrometer (FT-ICRMS), the sample ion motion in the magnetic field was used to analyze their mass to charge ratio, by measuring either the radius of trajectory or the frequency of the cyclotron motion in the magnetic field. Relying on high intensity and highly homogeneous magnetic field, the FT-ICRMS has unsurpassed mass measurement accuracy and resolution [1–4]. Briefly, the theoretical mass resolving power of FT-ICRMS for a fixed measuring time depends on the ion cyclotron motion frequency, and the frequency depends on the intensity of magnetic field. Therefore, increasing the intensity of magnetic field becomes one of the main goals of the instrumentation of FT-ICRMS, where the most advanced instrument is equipped with a superconducting magnet delivering the magnetic field in trapping area up to 21 Tesla [5, 6].

However, the majority of FT-ICRMS instruments with high intensity superconductor magnet are bulky, heavy, and costly. In order to reduce the weight and cost of superconductor magnets, Loreen C. Zeller in 1993 built a FT-ICRMS based on a 0.4 Tesla permanent magnet, and the device achieved a resolving power of 53,000 for very low mass ion (*m/z* 69) attributable to its limited magnetic induction intensity [7]. In recent years, substantial efforts have been made in the development of new magnetic materials that can give higher levels of stored magnetic energy. As a result, many reports on ICR device using permanent rear earth magnets appeared because they are small, inexpensive, and easy to maintain. In 2002, J.J. Jones and W.V. Rimkus in Siemens Applied Automation presented the first commercial FT-ICRMS with a 1 Tesla permanent magnet [8, 9]. In 2004, M. Heninger presented a Mobile Ion Cyclotron Resonance Analyzer (MICRA) based on a 1.24 Tesla permanent magnet weighing 40 kg, which remains compatible with genuine FT-ICRMS performance and a mass resolving power of 73,000 at mass 132 [10]. Nevertheless the practical utility of this instrument was limited by using internal ion sources or matrix-assisted laser desorption ionization (MALDI). In 2007, M.V. Gorshkov presented a FT-ICRMS based on a 0.97 Tesla permanent magnet weighing 37 kg. The device had an axial field that can utilize atmospheric pressure ionization methods such as electrospray ionization, and achieved a resolving power of 80,000 for the H_3O^+ ion and 25,000 with isotopically resolved mass spectra of peptides [11]. Although these instruments using permanent magnets showed

Correspondence to: Li Ding; *e-mail:* li.ding@srlab.co.uk, Chuan–Fan Ding; *e-mail:* cfding@fudan.edu.cn

reasonably good performances in terms of mass resolution, the ions they used are at low mass, and these devices are still heavy and bulky because large magnets were required to generate a uniform magnetic field in the full space of the ICR cell.

On the other hand, there is growing interests in design of FTMS using electrostatic field, such as the case of Orbitrap [12], where ions orbit around the central longitudinal electrode while the trajectories oscillate along the axis of the longitudinal electrode. By implementing the quadro-logarithmic field in the trap, the axial oscillation is harmonic and its frequency depends only on the mass to charge ratio but not orbital energy. Ions are injected from an external C trap to the Orbitrap and start the orbital and axial motion without further excitation in the Orbitrap. There are other types of electrostatic ion trap like linear electrostatic ion trap (LEIT) [13, 14] and pancake type electrostatic ion trap [15], which originated from the multiple reflection time-of-flight system to enlarge the space charge capacity. These trap devices also measure the image charge signal immediately after ions are injected into the trap without in-trap excitation.

Therefore, it is not necessary to provide homogenies magnetic field in the whole FT-ICR cell if ions are not resonantly excited from the center of the cell. If ions can be pre-accelerated outside the trap, homogenies magnetic field is only needed in the ion orbital region, so there is a possibility to downsize the magnets and reduce the size and weight of the total instrument.

In this paper, we propose a new type of orbital trap mass analyzer in which ions are confined by hybrid magnetic and electric field. The hybrid magnetic-electric field orbital trap (MEOT) is different from conventional FT-ICRMS in that ions are injected directly into the annular orbital space by a pulsed high voltage without exploiting excitation of ions from center to larger radius by cyclotron resonance excitation. Because no cyclotron resonance excitation is used, the uniform magnetic field is only required in an annular space and the size of the magnet can be smaller than previously reported. The trap analyzer performs mass analysis using imagining charge/current pickups and FFT method. This paper presents the concept of the design and using simulation proves the working principle, and optimizes some key parameters of the device.

Configuration of the Hybrid Magnetic-Electric Field Orbital Trap

The structural diagram of MEOT is shown in Figure 1. Figure 1a shows the complete structure, including mass analyzer and ion injection system, and Figure 1b shows the mass analyzer with proposed magnet structure in exploded view. The cross-section of the designed assembly diagram with the permanent magnets is shown in Figure 1c. The magnet is composed of a center cylindrical piece and top and a bottom discs, forming an annular field gap between the top and bottom discs. The annular space in the gap provides a strong magnetic field to trap ions flying with the circular orbit, with the magnetic flux perpendicular to the ions' circular orbits.

Surrounding the annular orbiting space, there are two sets of sector focusing electrodes on each side of the orbiting space, and one outer ring electrode and one inner ring electrode to provide electrostatic focusing field. The confinement by the magnetic field in radial direction and focusing by the electrostatic field in both radial and axial directions keep the ion orbiting inside the annular space without escaping in either direction. The outer ring electrode has an inner diameter of 39 mm, and the voltage is set 0 V. The inner ring electrode has an outer diameter of 31 mm, and is applied with a low negative voltage, which will be discussed in detail in the following part.

There are 24 identical sector plates in each set in Figure 1, but they can be other even numbers and subject to optimization. The distance between the two opposite identical sector plates is 10 mm in z direction. All odd-numbered sector plates (in both top and bottom sets) are connected and supplied with voltage +V, whereas all even-numbered sectors are connected and supplied with voltage –V. These sector electrodes also act as image charge pickup electrodes so all charge gathered by even-numbered sectors and by odd-numbered sectors are differentially coupled to the signal amplifier, as shown in Figure 2.

The outer ring electrode has a 4 mm × 10 mm slit for receiving injected ions. The ion injection system, as shown in Figure 1a, is mainly composed of a small linear ion trap (in rectlinear ion trap [16] configuration with its axis in y direction) and an ion transferring optical system, which includes three pairs of focusing plates applied with different DC voltages for focusing of ions during injection. With proper voltage arrangement to the optical system, the sample ions that were generated outside of the magnetic field region can be injected tangentially into the annular orbital flight path.

As shown in Figure 1, the key difference of the magnet setup between MEOT and traditional FT-ICR is that only uniform magnetic field in the annular orbital space is formed, and thus the total magnetic flux is reduced and a smaller/lighter permanent magnet can be used.

The sample ions created in any ion source were first transmitted through an intermediate vacuum ion guide (not shown in Figure 1) to the rectlinear ion trap where ions can be accumulated and cooled. The linear trap has a rectangular cross-section of 10 × 10 mm. After a while, a pulsed high voltage of ion injection is applied to one of the x plates, which is marked as the injection plate in Figure 1, and all ions are pushed into a differentially pumped region, which has three pieces of focusing plates by the pulsed voltage. Therefore, ions can be accelerated to a certain momentum before entering the annular orbital region.

The ions start the cyclotron motion once they enter the magnetic field in the annular trapping region. As shown in Figure 2, the imaging charge/current is produced while ions pass through each pair of sector electrodes during their cyclotron motion. These oscillating image charge signals will be coupled to the amplifier via DC isolation capacitors and be amplified and recorded. Using fast Fourier transformation (FFT), the signal is then converted and displayed as a mass spectrum.
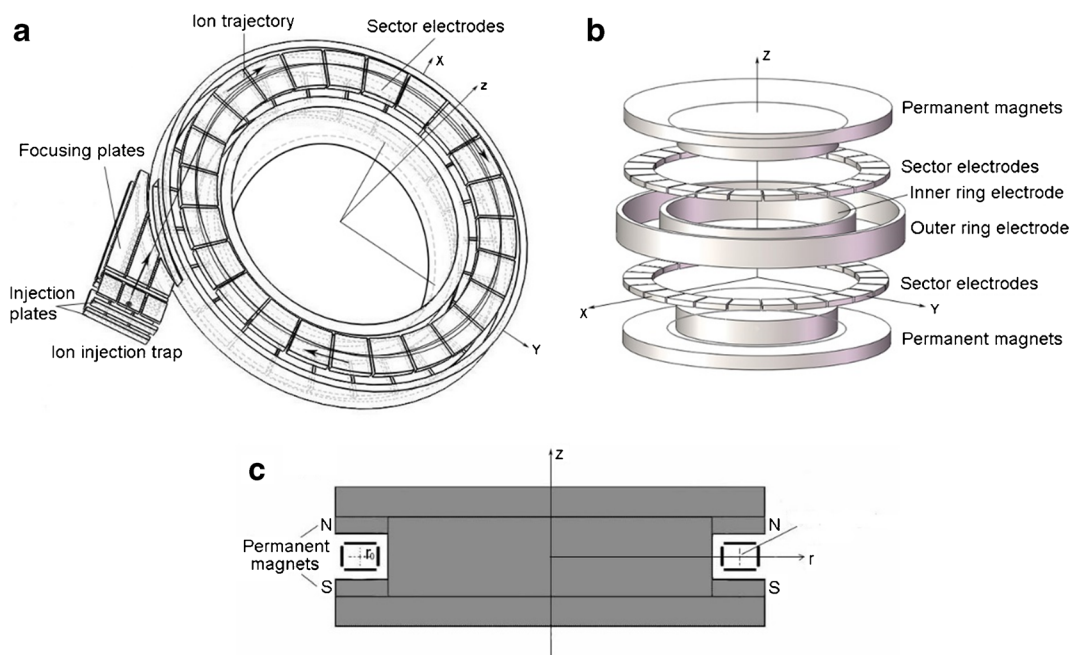
Figure 1. Schematic presentation of the MEOT mass analyzer: **(a)** shows the complete structure including mass analyzer and its ion injection system, **(b)** shows the main part of MEOT mass analyzer with magnetic field in exploded view: two identical sector electrodes, one outer ring electrode, one inner ring electrode, and the annular permanent magnets for ion cyclotron motion, **(c)** is the cross-section of the designed assembly diagram with the permanent magnets

Working Principle in Details

Injection Condition

Instead of utilizing resonance excitation typically used in the ICR cell, ions should be pre-accelerated and injected into the annular orbital space from an ion source. During the ion motion in the MEOT, the tangential velocity v of ion satisfies the centripetal force balance:

$$F = qvB = \frac{mv^2}{R_0} \tag{1}$$

Here, B is the magnetic induction intensity, m and q are mass and charge of the ion, respectively, and R_0 is the radius of the ion orbital motion; therefore we have

$$mv = qBR_0 \tag{2}$$

Equation 2 shows that the momentum of different ions with the same charge entering the orbit with certain radius a constant

for a constant magnetic field B. Assuming that all ions in the ion source (or an ion storage device) have initial zero or negligible kinetic energy, the injection process must consist of acceleration with a constant impulse to the injected ions. Such acceleration may be achieved by a short pulsed but high intensity electric field. The field intensity E_{ac} and its duration Δt must satisfy

$$E_{ac} \Delta t = BR_0 \tag{3}$$

This injection method is different from those used in other mass spectrometers, such as in time-of-flight (TOF) mass spectrometer or electrostatic Orbitrap mass analyzer, where constant energy acceleration is employed. During injection, ions will be inevitably deflected by the magnetic field diffused in the injection path. Therefore, an additional temporary magnetic field generated by a coil in opposite polarity will be superimposed to the permanent magnetic field to substantially neutralize the magnetic field in the space of injection path. The technology for generating short pulsed
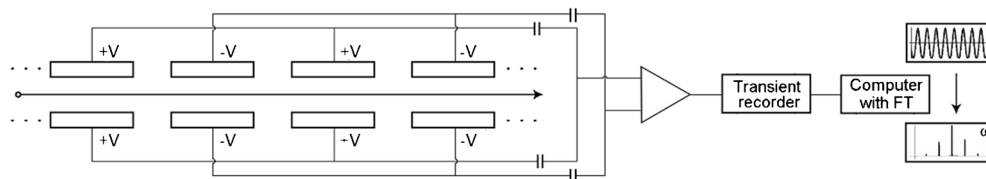
Figure 2. Every other one of the 24 sector plates were electrically connected together to form two groups of electrodes. One group was applied with +V, and another group was applied with –V. Imaging charge/current will be produced when ions pass through each pair of sector electrodes and capacitively coupled to the low noise amplifier before recorded and converted by FFT

strong magnetic is available [17, 18] but detailed design is not presented in this paper.

Frequency Compensation

When initial lateral kinetic energy (in direction z, in Figure 1a) is controlled to be very small, a very small voltage +/–V on the sector electrodes to keep ions stable within the annular orbital space contributes to only minor modification to the cyclotron frequency. The angular frequency of the ion motion is approximately the cyclotron frequency:

$$\omega \approx B\left(\frac{m}{q}\right)^{-1} \tag{4}$$

However, the electric focusing field is necessary to keep the ion in the annular orbit and it does affect the angular frequency of ion motion to a certain extent. The extent of influence may vary depending on the location of the ion, so the isochronous performance of ion motion should be studied carefully. In the current design, the focusing electric field is formed by the sector electrodes of alternately changed polarities along the ion's orbit. Ions, after being tangentially injected into the circular orbit with radius R_0, subject a varying focusing electric field, which focuses them to the center orbit (*radius* $\rho = R_0$, z = 0). This electric field consists of mainly quadrupole field component while other high order field components also exist. As an approximation, the force from the varying quadrupole field is used to estimate the influence in radial direction, and the effective radial force can be expressed as

$$F_\rho = eE_{eff} = -\alpha eV(\rho - R_0) \tag{5}$$

Where where E_{eff} is the effective dynamic focusing field caused by the alternating DC voltage V on the sector electrodes (for example V= V_2= $-V_4$ = 2 V in following the discussion), and has approximately linear relation with the relative radial displacement $\rho - R_0$. The force is centripetal when $\rho > R_0$ but centrifugal when $\rho < R_0$. Here, the coefficient α is a function of the ion's linear velocity and inscribes radius r_0 of the quadrupole field in the annular space. The detailed investigation of the dynamic focusing and the derivation of coefficient α will be published separately.

When ion moves on a circular orbit defined by both Lorentzian force and electrical force,

$$m\omega^2\rho = Be\omega\rho - eE_{eff} = Be\omega\rho + \alpha eV(\rho - R_0) \tag{6}$$

$$m\omega^2 - Be\omega - \alpha eV + \frac{\alpha eVR_0}{\rho} = 0 \tag{7}$$

If without last term, the equation becomes independent of ρ, so the solution is,

$$\omega = \frac{Be + \sqrt{B^2e^2 + 4me\alpha V}}{2m} \tag{8}$$

It is independent of radius ρ, or flying energy. When the last term of Equation 7 is considered, it reduces the centripetal force; hence its existence causes a ρ-dependent reduction of the frequency. The larger the ρ, the smaller the reduction (higher ω), so the desired isochronous is lost. The problem can be solved by adding a constant centripetal force in Equation 6 to cancel the last term. In order to achieve this, we apply a negative voltage V_1 on the inner ring electrode while keeping the outer ring electrode at 0 V. Such an inward dipole field only slightly shifts up the angular velocity of the ion. As shown in the following section, a –0.01 V on the inner ring electrode gives the trap good isochronous performance and increases the rotation frequency only by 2 Hz (from 52 kHz).

Ion Imaging Charge/Current Pickup

To increase the resolving power in the FT-ICRMS, multiple electrode detection systems for enhancing high harmonics in signal was first implemented by Nikolaev [19]. In MEOT, the imaging charge/current will be produced when the ion passes by neighboring electrodes, as shown in Figure 2. When there are 24 pairs of sector electrodes, one ion cyclotron motion will produce 12 waves of imaging charge/current signal. The frequency of the image charge signal of MEOT is therefore 12 times the frequency of the ion's cyclotron motion. In a normal FT-ICRMS, one cyclotron motion will produce only one wave of imaging charge/current signal, so the newly designed MEOT can achieve 12 times higher signal frequency for a certain mass of ion compared with a conventional FT-ICR mass analyzer at the same magnetic induction intensity. This in turn can improve the ultimate mass resolving power or reduce the data acquisition time. The larger the number of sector electrodes used, the larger the boost to the signal frequency. However, when the interval between the two neighboring sector electrodes becomes too small (equal or smaller than the distance between of two end sets), the intensity of the image charge signal picked up by the electrodes will reduce. This sets the upper limit for the number of sector electrode used.
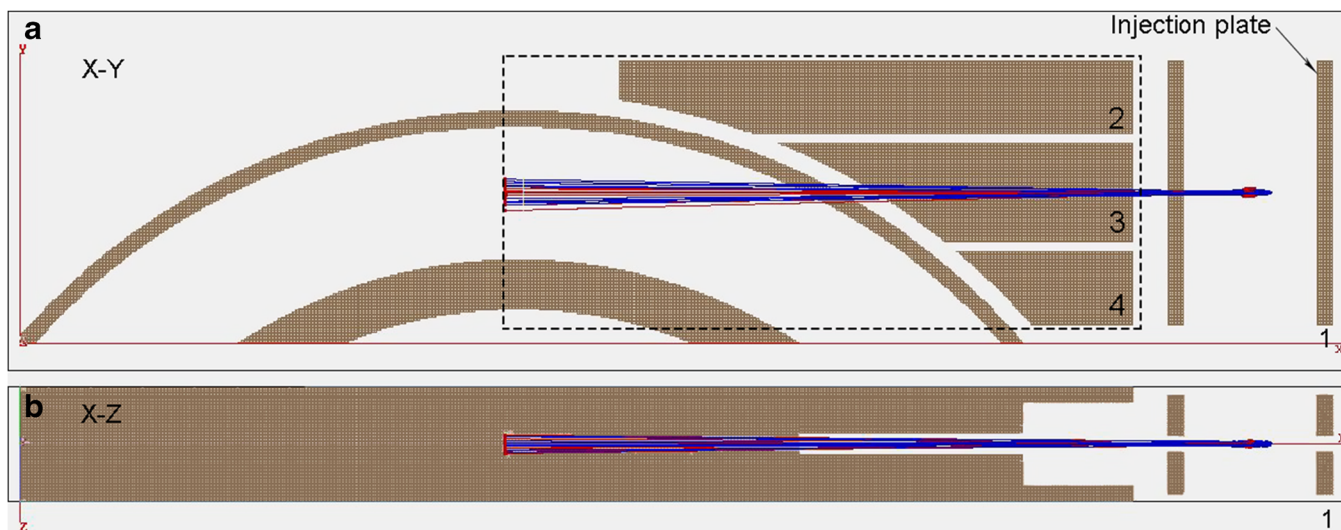
Simulations

Platforms

Owing to the limit of computer memory, the field regions of MEOT and ion introduction system are simulated separately, so there were two work benches used in the simulations, both using SIMION 8.1 [20]. One contained a cylindrical magnetic field region and a 3D planar electric field region for simulating the annular magnetic and electric trapping as shown in Figure 1b. The 800 × 800 × 100 units potential array only

Table 1. Ions of 400 Th and 1000 Th initial phase space parameters before injected into the orbital trap

| m/z	Phase space coordinates	x(mm)	y(mm)	z(mm)	E_x (eV)	E_y (eV)	E_z (eV)
400	Mean value	43.98	35.02	0.017	0.13	0.086	0.11
	Std Dev	0.053	0.039	0.024	0.091	0.025	0.042
1000	Mean value	44.07	35.02	0.020	0.07	0.069	0.09
	Std Dev	0.017	0.021	0.029	0.059	0.019	0.021

Figure 3. Simion screen captures **(a)** in the XY plane, **(b)** in the XZ plane, during simulation of ion injection through the focusing plates and the slit in the outer ring electrode. Ions of 400 Th are in blue and 1000 Th are in red). The dashed frame shows the additional temporary magnetic field region to substantially neutralize the magnetic field in the space of injection path. Some electrodes and the slit on outer ring electrode are hidden to show the ion trajectories clearly

covers the space in first octant of the annular space with the resolution of 0.05 mm per grid unit. This array was mirrored in x, y, z directions to produce the work bench covering the entire annular space with maximum diameter of 80 mm and thickness of 10 mm. Another one contained a 3D field region for simulating ion introduction. The potential array resolution was 0.05 mm per grid unit and the size was $1600 \times 350 \times 200$. The fields in all these field regions were calculated using SIMION 8.1 and the results were saved as adjustable PA files. Because both the MEOT and its ion introduction system used flat surface electrodes, the finite differential method with cubical grid for field calculation in SIMION 8.1 can give accurate result, as long as all conductor surfaces run through the grid nods. A user program was prepared in "Lua" to control the parameter exchange and ray tracing and to record the image charge signal during the simulation.

Ion Injection

In the simulations of ion injection, sample ions were generated outside the magnetic field region, and readily stored in the linear ion trap driven by digital high frequency signal. The digital waveform is easier to be implemented in simulation program, and the associated switching circuit is also practically compatible to the circuit making pulsed injection signal at one
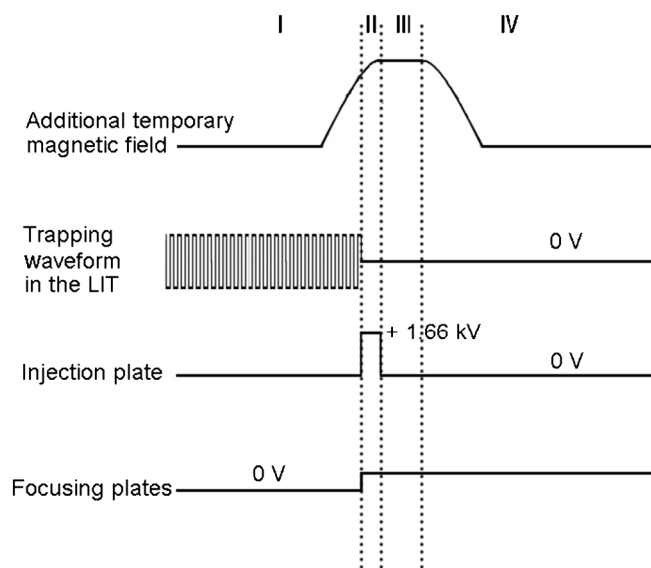
I. Pre-Ionization and cooling for 5 ms
II. Injection, 0.1 μs
III. Ion transfer to the X = 0 plane, 20 μs
IV. Trapping in the MEOT

Figure 4. Time sequences of ion injection using the additional temporary magnetic field

Table 2. Ions of 400 Th and 1000 Th phase space parameters after injected into the orbital trap when stopped at the X = 0 plane of orbital space

m/z	Phase space coordinates	x(mm)	y(mm)	z(mm)	E_x (eV)	E_y (eV)	E_z (eV)
400	Mean value	−0.022	35.08	0.32	35.04	0.019	0.035
	Std Dev	0.012	0.37	0.48	0.63	0.016	0.023
1000	Mean value	−0.017	34.99	−0.49	14.02	0.027	0.026
	Std Dev	0.014	0.42	0.33	0.42	0.014	0.013

of the x plates. Previously people have studied the distribution of the cooled ion cloud in the favorite wave phase in the linear quadrupole ion guide driven by digital square wave [21]. In the current simulation, we assumed that a group of ions of different mass to charge ratio were first thermalized in a linear ion trap with a buffer gas of room temperature and pressure of 0.13 Pa. The linear ion trap was driven with a 990 KHz, 0-p 390 V high frequency square wave voltage. The voltage on two end caps of the linear ion trap was set at 150 V. Phase space distributions in x, y, and z directions can be obtained after the simulating with cooling time of 9 ms, sampled at middle phase of positive half of the square wave. Ions cooled to the middle of the linear ion trap achieved pre-injection conditions listed in the Table 1.

In Equation 2 and Equation 3, the momentum of different ions is a constant for a constant magnetic induction intensity, and the injection process must consist of acceleration with a constant impulse to the injected ions. During the ion injection period, the square wave stopped and a short pulse of 0.1 μs and 1.66 kV was applied on the injection plate (Electrode 1) of the linear ion trap as shown in Figure 3a. As previously mentioned and shown in Figure 3, the dashed frame shows the additional temporary neutralization magnetic field region, which was implemented for ion injection. The time sequences in this study are shown in Figure 4. Through the focusing plates, 40 ions of 400 Th and 40 ions of 1000 Th were injected tangentially into the annular orbital flight path. In the simulation, the voltages of the focusing plates (Electrode 2, Electrode 3, and Electrode 4) were set at +0.6 V, +0.4 V, +0.6 V, respectively, from top to bottom. The velocity and position information of ions was recorded by user program when they arrived at the X = 0 plane of the orbital space, achieving the phase space parameters listed in the Table 2. Figure 3 shows the ion trajectories after injection in XY and XZ planes. Note that the momentum in x diretion for two ions of different mass $mv = \sqrt{2E_x m}$ remain the same.

Ion Trapping

This work bench contained a cylindrical magnetic field region and the magnetic induction intensity was 0.5 to 1 Tesla. In this work bench, the inner ring electrode was made solid (filled with electrode in SIMION) in order to save time of refining procedure.

In the first simulation, 40 ions of 400 Th and 40 ions of 400.1 Th were injected into the orbital space. The values of ion motion parameters were copied from the file recorded by the user program in the first work bench. In order to achieve a circular orbital trajectory, the initial E_x values of ions of 400 Th for different magnetic induction intensity are listed in Table 3.

From the simulation, it was found that for 0.5 Tesla the optimized voltage on the inner ring electrode was −0.01 V and the outer ring electrode was 0 V. There are sector electrodes on each side surrounding the flight path to restrict the ion motion in the axial direction. The voltages on the sector electrodes were set at +/− 2 V alternately between two adjacent sectors.

The motion of ions induced image charges on the sector pickup electrodes and changed their potentials. The change in potentials on sector electrodes was recorded by our user program and it is considered as an image charge signal. Figure 5 shows the ion trajectories in XY plane and XZ plane. The ions of 400 Th, which are marked in green, fly faster than ions of 400.1 Th because ions of lower mass have higher orbital frequency in the hybrid magnetic-electric field. Moreover, ions can be trapped in axial direction because of the alternating arranged DC voltages on the sector electrodes.

When ions fly in the annular flight path surrounded by the +/− 2 V sector plates, they "see" an equivalent trapping "rf" field in both axial and radial directions. It is worth mentioning that the effective potential well depth is relatively small with only +/− 2 V setting but the reason the ions can be trapped may be attributable to the high order field. The ions' circular orbits can be approximated as a quadrupole field if ion is close to the axis of fly path (r = R_0, z = 0), but when ion flies away from the axis, there is a significant amount of high order field component, which gives much higher focusing force than a quadrupole field. Figure 5b shows that as the ion trajectory reaches the edge of the tunnel, being quite close to the sector electrodes, provides sufficient accumulated return force to the ions.

Table 3. The required E_x for ions of 400Th under different magnetic induction intensity at the X = 0 plane of orbital space

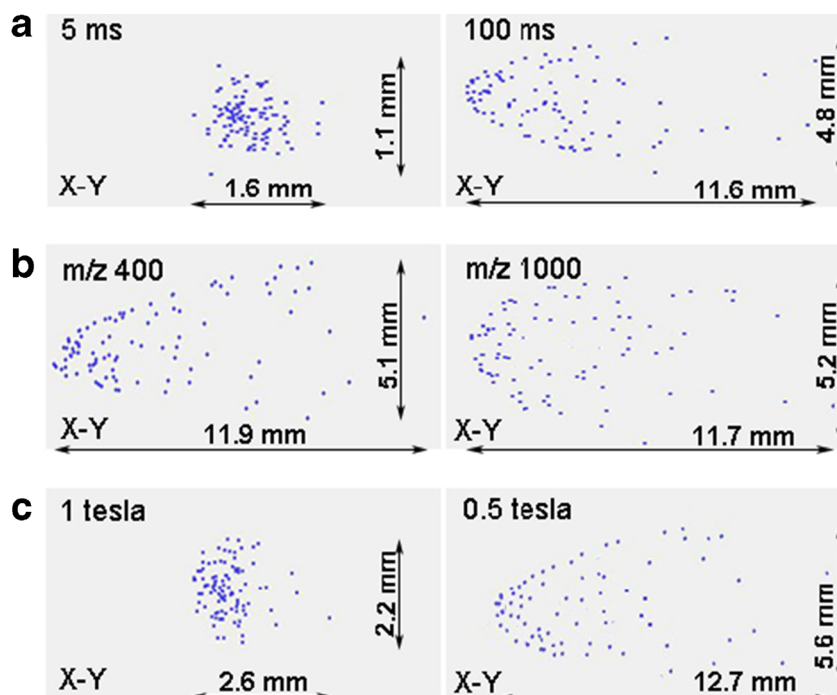| Magnetic induction intensity (Tesla)	0.5	0.6	0.7	0.8	0.9	1.0
E_x (eV)	35.04	52.98	71.81	94.16	119.08	147.03
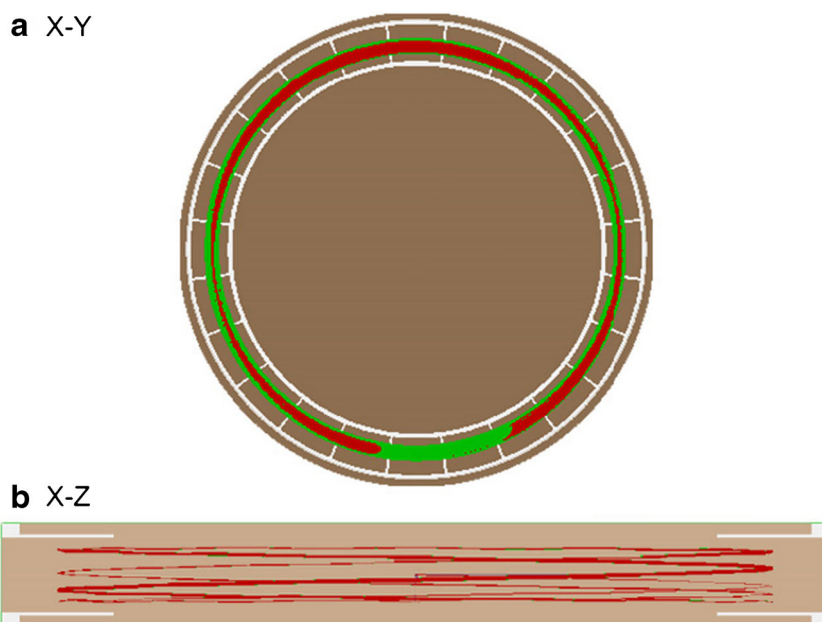
Figure 5. Ion trajectories and ion cloud distribution for ions of 400 Th (green color) and 400.1 Th (red color) in **(a)** XY plane and in **(b)** XZ plane, the magnetic induction intensity is 0.5 Tesla

Results and Discussions

Ion Cloud Dephasing and "Comet" Structure Formation

In the FT-ICRMS with spatially homogeneous magnetic field, ions synchronized during cyclotron excitation continue to be in synchronous motion indefinitely in the absence of collisions with neutrals and ion–ion interactions [22, 23]. The existence of superimposed electric field causes magnetron motion and the inhomogeneity of the field results in ion cloud dephasing and "comet" structure formation.

Figure 6. Destruction of an ion cloud in the MEOT from the view of XY plane. **(a)** Shows the effect of different time of motion (*m/z* is 400, magnetic induction intensity is 0.5 Tesla, 5 ms versus 100 ms); **(b)** shows the effect of different *m/z* (time is 120 ms, magnetic induction intensity is 0.5 Tesla); **(c)** shows the effect of different magnetic induction intensity *m/z* is 400, time of motion is 150 ms, 1 Tesla versus 0.5 Tesla)
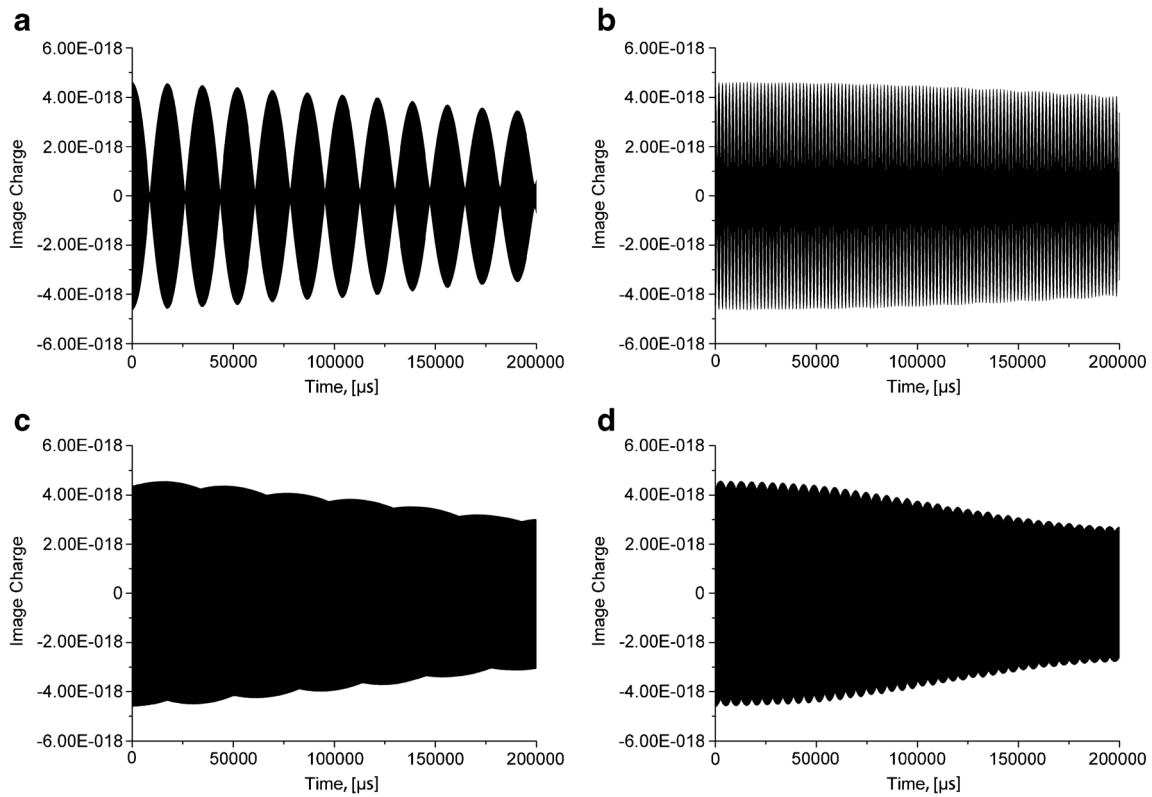
Figure 7. Image charge signals of 200 ms acquired in simulation from the 12 pairs of sector electrodes. (the magnetic induction intensity is 0.5 Tesla)
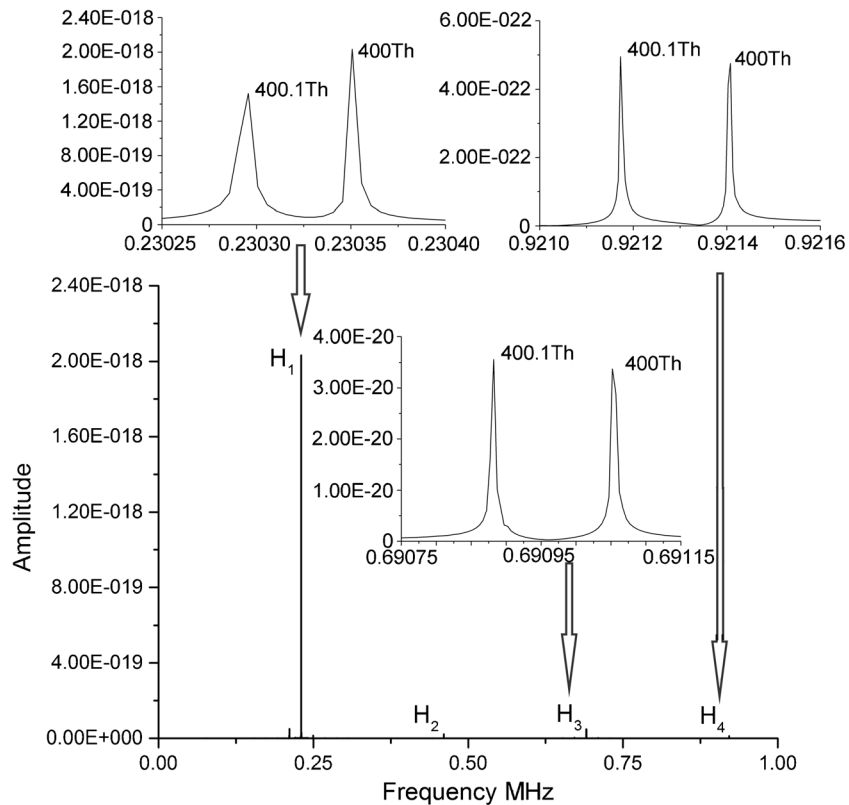

Figure 8. FFT spectrum for the image charge signal from the 12 pairs of sector electrodes, with insertions showing the zoom-in spectra localized around 1st, 3rd, and 4th harmonic peak group. Hann window has been used (the magnetic induction intensity is 0.5 Tesla and the flight time is 200 ms)

Table 4. The optimized V_1 for different values of V_2

V_2 (V)	1.0*	1.2	1.6	1.8	2.0
V_1 (V)	−0.0036	−0.0047	−0.0049	−0.0049	−0.0050
V_2 (V)	2.2	2.4	2.8	3.6	4.4
V_1 (V)	−0.0051	−0.0052	−0.0054	−0.0063	−0.0088

*When the value of V_2 is set less than 1.2 V, there are ion losses by hitting the sector focusing electrode. Therefore the mass resolving power is not accurate when the value of V_2 is 1.0 V.

In the simulation of the MEOT, ion cloud dephasing was also observed as a result of different z-oscillation amplitudes. Figure 6a shows the same type of ions of 400 Th for a constant magnetic induction intensity of 0.5 Tesla. Simulation shows that a longer time of motion leads to larger ion cloud destruction. In Figure 6b, different ions of 400 and 1000 Th orbit in the same magnetic induction intensity of 0.5 Tesla. After a certain time of simulation, the rates of ion cloud destruction in tangential direction are the same for clouds of different -m/z. Figure 6c shows the ion of 400 Th in different magnetic induction intensity from 0.5 to 1 Tesla. After a certain time of simulation, the rate of ion cloud destruction is lower for the higher magnetic induction intensity. It can be concluded that an increase in the magnetic field would increase the resolving power.

The Image Charge Signals

The image charge of all ions flying in the MEOT can be recorded utilizing the user program in SIMION 8.1. In the simulation, 12 pairs of sector focusing electrodes also play the role of picking up image charge. Figure 7 shows the transient signals acquired in two separate simulations for 200 ms. The decay of the signal to 73% was attributable to the ion cloud spreading out rather than the ion loss by hitting the electrodes. Figure 7a has 40 ions of 400 Th and 40 ions of 400.1 Th, Figure 7b has 40 ions of 400 Th and 40 ions of 401 Th, Figure 7c has 40 ions of 400 Th and 40 ions of 500 Th, and Figure 7d has 40 ions of 400 Th and 40 ions of 1000 Th.

Simulated Mass Resolution

The Fourier transform to the image charge signals is displayed in Figure 8. There is more than one harmonic frequency component existing in the spectrum, but the amplitude is relatively low. Therefore Figure 8 just shows the harmonic components H_1 to H_4. Note that the fundamental frequency (H_1) is already 12 times the ion orbital frequency in the MEOT. As shown by the insertions, each of the harmonic components (from H_1 to H_4) is capable of separation of the two ions with m/z 400 and 400.1 Th after 200 ms, although the higher harmonic components produce better mass resolution. The FWHM of H_1, H_3, and H_4 peaks are calculated and mass resolving powers of 37, 60, and 79 k were achieved, respectively, at the 0.5 Tesla magnetic induction intensity.

Moreover, the magnetic induction intensity was changed in this simulation study from 0.5 to 1 Tesla. In the FT-ICRMS, it is accepted that resolving power is

$$RP = m/\Delta m = \omega/\Delta\omega \qquad (9)$$

In this equation, $\Delta\omega$ denotes the width of the peak in the frequency domain spectra and Δm denotes the width of the peak in the mass spectrum. In Equation 9, because ω is proportional to magnetic field B and $\Delta\omega$ is inversely proportional to observation time, R should linearly increase with B. Supplementary Figure S1 shows the simulated resolving power at different magnetic induction intensities. The simulated mass resolving power up to 72 k was achieved and it does linearly increase with the magnetic field used.

In Equation 5, E_{eff} is the effective dynamic focusing field as ions alternately experience the reversed DC potential created by the sector electrodes. In the simulation, different values of DC voltage V were applied on the sector electrodes and the change of resolving power was observed. According to the Equation 7 and Equation 8, a negative voltage V_1 on the inner ring electrode should be applied to counteract the last term in Equation 7 and retain good isochronous performance. Supplementary Figure S2 shows the simulated resolving power at different alternating DC voltages on the sector electrodes along with its optimized V_1. In the simulation, we set the value of V_2 and changed different values of V_1 to get the best mass resolution. The values of V_1 for different values of V_2 are listed in Table 4. The DC voltage changed from 1.0 to 4.4 V, and the resolving power peaked at 2 V.

Conclusions

The hybrid orbital trap mass analyzer applied with both magnetic and electric field (MEOT) can be designed with a rotational symmetrical structure. While it shares the rotational symmetrical feature with the FT-ICR, it differs from the arrangement of magnet and image charge signal pickups. Ions will be injected directly into the annular space of the analyzer without being excited from center to a larger radius by cyclotron resonance excitation, so it provides a way to downsize the magnets and reduce the size and weight of the total instrument. Because there are 24 electrodes and each pair of neighboring

electrodes will give one image charge/current "pulse" when ion cloud passes through, 12 pulses are generated in one circular motion of ions; therefore the newly designed hybrid orbital trap can deliver 12 times higher signal frequency for a certain mass of ion compared to a conventional FT-ICR mass analyzer with the same magnetic intensity. Thus it can improve the ultimate mass resolving power or reduce the data acquisition time.

Mass resolution (FWHM) of more than 79,000 at magnetic induction intensity of 0.5 Tesla has been obtained in the simulation after optimization. The simulated mass resolving power linearly increases with the intensity of magnetic field and the alternating DC voltage on the sector electrodes also affects the resolving power.

The ion injection is based on the constant momentum acceleration in tangential direction and a temporary neutralization magnet is proposed to increase the injection efficiency. Further simulation to refine the structure and design a more practical injection system will be carried out.

It is worth stating that the current simulation has not taken into account any ion collision with the residual gas molecules. For the orbital time up to 200 ms and a vacuum degree better than 1×10^{-8} mbar, such an assumption is valid. For a poorer vacuum or longer orbiting time, the behavior of ion cloud would be different from those in a ICR cell, as ions may suffer a "sudden death" after an ion-molecule collision and hit the inner ring electrode. Such special aspects will be our future topics of study. Of course we also plan to set up experiments to prove the result of simulation.

Acknowledgment

References

1. Marshall, A.G., Hendrickson, C.L., Jackson, G.S.: Fourier transform ion cyclotron resonance mass spectrometry: a primer. Mass Spectrom. Rev. **17**, 1–35 (1998)
2. Bogdanov, B., Smith, R.D.: Proteomics by FTICR mass spectrometry: top down and bottom up. Mass Spectrom. Rev. **24**, 168–200 (2005)
3. Marshall, A.G., Guan, S.: Advantages of high magnetic field for fourier transform ion cyclotron resonance mass spectrometry. Rapid. Commun. Mass Spectrom. **10**, 1819–1823 (1996)
4. Dienes, T., Pastor, S.J., Schürch, S., Scott, J.R., Yao, J., Cui, S., Wilkins, C.L.: Fourier transform mass spectrometry-advancing years (1992 to mid-1996). Mass Spectrom. Rev. **15**, 163–211 (1996)
5. Nikolaev, E.N., Jertz, R., Grigoryev, A., Baykut, G.: Fine structure in isotopic peak distributions measured using a dynamically harmonized Fourier transform ion cyclotron resonance cell at 7 T. Anal. Chem. **84**, 2275–2283 (2012)
6. Hendrickson, C.L., Quinn, J.P., Kaiser, N.K., Smith, D.F., Blakney, G.T., Chen, T., Marshall, A.G., Weisbrod, C.R., Beu, S.C.: 21 Tesla Fourier transform ion cyclotron resonance mass spectrometer: a national resource for ultrahigh resolution mass analysis. J. Am. Soc. Mass Spectrom. **26**, 1626–1632 (2015)
7. Zeller, L.C., Kennady, J.M., Kenttamaa, H., Campana, J.E.: Characterization of a small FT-ICR mass spectrometer based on a permanent magnet. Anal. Chem. **65**, 2116–2118 (1993)
8. Jones, J.J., Wilkins, C.L. Bacterial pyrolysis products analyzed using a portable high resolution 1 Tesla Fourier transform mass spectrometer. Proceedings of the 52nd ASMS Conference on Mass Spectrometry and Allied Topics, Nashville, TN (2004)
9. Rimkus, W.V., Davis, D.V., Gallaher, K. Learn FTMS fundamentals and quantitation on an inexpensive rugged machine—save your high powered FTMS for the experienced user. Proceedings of the 53rd ASMS Conference on Mass Spectrometry and Allied Topics, San Antonio, TX (2005)
10. Mauclaire, G., Lemaire, J., Boissel, P., Bellec, G., Heninger, M.: MICRA: a compact permanent magnet Fourier transform ion cyclotron resonance mass spectrometer. Eur. J. Mass Spectrom. **10**, 155–162 (2004)
11. Vilkov, A.N., Gamage, C.M., Misharin, A.S., Doroshenko, V.M., Tolmachev, D.A., Tarasova, I.A., Gorshkov, M.V.: Atmospheric pressure ionization permanent magnet Fourier transform ion cyclotron resonance mass spectrometry. J. Am. Soc. Mass Spectrom. **18**, 1552–1558 (2007)
12. Makarov, A.: Electrostatic axially harmonic orbital trapping: a high performance technique of mass spectrometry. Anal. Chem. **72**, 1156–1162 (2000)
13. Benner, W.H.: Gated charged particle trap. US patent No. 5880466, March 9 (1999)
14. Zajfman, D., Rudich, Y., Sagi, I., Strasser, D., Savin, D.W., Goldberg, S., Rappaport, M., Herber, O.: High resolution mass spectrometry using a linear electrostatic ion beam trap. Int. J. Mass Spectrom. **229**, 55–60 (2003)
15. Ding, L., Badheka, R., Ding, Z.T., Nakanishi, H.: A simulation study of the planar electrostatic ion trap mass analyzer. J. Am. Soc. Mass Spectrom. **24**, 356–364 (2013)
16. Song, Q., Kothari, S., Senko, M.A., Schwartz, J.C., Amy, J.W., Stafford, G.C., Cooks, R.G., Ouyang, Z.: Rectilinear ion trap mass spectrometer with atmospheric pressure interface and electrospray ionization source. Anal. Chem. **78**, 718–725 (2006)
17. Xu, Y., Yang, R., Xiang, Y., Ding, H., Ding, T., Li, L.: Design of a novel pulsed power system for repetitive pulsed high magnetic fields. IEEE Trans. Appl. Supercond. **22**, 5400104–5400104 (2012)
18. Kohama, Y., Kindo, K.: Generation of flat-top pulsed magnetic fields with feedback control approach. Rev. Sci. Instrum. **86**, 104701 (2015)
19. Nikolaev, E.N., Rakov, V.S., Futrell, J.H.: Analysis of harmonics for an elongated FTMS cell with multiple electrode detection. Int. J. Mass Spectrom. Ion Processes. **157/158**, 215–232 (1996)
20. Manura, D.J., Dahl, D.A.: SIMION v.8.1. Scientific Instrument Services Inc. / Idaho National Laboratory (2011)
21. Giles, R., Rousell, D., Sudakov, M., Papanastasiou, D.: An investigation into digital ion trap as an ion source for a time of flight instrument. Poster Press, ASMS 55, June, MPC040 (2007)
22. Nikolaev, E.N., Kostyukevich, Y.I., Vladimirov, G.N.: Fourier transform ion cyclotron resonance (FT-ICR) mass spectrometry: theory and simulations. Mass Spectrom. Rev. **35**, 219–258 (2016)
23. Nikolaev, E.N.: Some notes about FT-ICR mass spectrometry. Int. J. Mass Spectrom. **377**, 421–431 (2015)